IGF2BP2 Maintains Retinal Pigment Epithelium Homeostasis by Stabilizing *PAX6* and *OTX2*

Siqi Wu,[1] Fuxi Li,[2] Kunlun Mo,[1] Huaxing Huang,[1] Yankun Yu,[3] Ying Huang,[1] Jiafeng Liu,[1] Mingsen Li,[1] Jieying Tan,[1] Zesong Lin,[1] Zhuo Han,[1] Li Wang,[1] and Hong Ouyang[1,4]

[1]State Key Laboratory of Ophthalmology, Zhongshan Ophthalmic Center, Sun Yat-Sen University, Guangdong Provincial Key Laboratory of Ophthalmology Visual Science, Guangzhou, China
[2]Guangdong Provincial People's Hospital, Guangdong Academy of Medical Sciences, Guangzhou, China
[3]Department of Pathology, The First Affiliated Hospital of Shihezi University, Shihezi, Xinjiang, China
[4]Center for Stem Cell Biology and Tissue Engineering, Key Laboratory for Stem Cells and Tissue Engineering, Ministry of Education, Zhongshan School of Medicine, Sun Yat-Sen University, Guangzhou, China

Correspondence: Hong Ouyang, State Key Laboratory of Ophthalmology, Zhongshan Ophthalmic Center, Sun Yat-Sen University, Guangdong Provincial Key Laboratory of Ophthalmology Visual Science, Guangzhou 510060, China;
ouyhong3@mail.sysu.edu.cn.
Li Wang, State Key Laboratory of Ophthalmology, Zhongshan Ophthalmic Center, Sun Yat-Sen University, Guangdong Provincial Key Laboratory of Ophthalmology Visual Science, Guangzhou 510060, China;
wangli59@mail.sysu.edu.cn.

Received: February 19, 2024
Accepted: May 15, 2024
Published: June 11, 2024

Citation: Wu S, Li F, Mo K, et al. IGF2BP2 maintains retinal pigment epithelium homeostasis by stabilizing *PAX6* and *OTX2*. *Invest Ophthalmol Vis Sci.* 2024;65(6):17. https://doi.org/10.1167/iovs.65.6.17

Purpose. N^6-methyladenosine (m^6A) methylation is a chemical modification that occurs on RNA molecules, where the hydrogen atom of adenine (A) nucleotides is replaced by a methyl group, forming N^6-methyladenosine. This modification is a dynamic and reversible process that plays a crucial role in regulating various biological processes, including RNA stability, transport, translation, and degradation. Currently, there is a lack of research on the role of m^6A modifications in maintaining the characteristics of RPE cells. m^6A readers play a crucial role in executing the functions of m^6A modifications, which prompted our investigation into their regulatory roles in the RPE.

Methods. Phagocytosis assays, immunofluorescence staining, flow cytometry experiments, β-galactosidase staining, and RNA sequencing (RNA-seq) were conducted to assess the functional and cellular characteristics changes in retinal pigment epithelium (RPE) cells following short-hairpin RNA–mediated knockdown of insulin-like growth factor 2 mRNA-binding protein 2 (IGF2BP2). RNA-seq and ultraviolet crosslinking immunoprecipitation with high-throughput sequencing (HITS-CLIP) were employed to identify the target genes regulated by IGF2BP2. adeno-associated virus (AAV) subretinal injection was performed in 6- to 8-week-old C57 mice to reduce IGF2BP2 expression in the RPE, and the impact of *IGF2BP2* knockdown on mouse visual function was assessed using immunofluorescence, quantitative real-time PCR, optical coherence tomography, and electroretinography.

Results. IGF2BP2 was found to have a pronounced effect on RPE phagocytosis. Subsequent in-depth exploration revealed that IGF2BP2 modulates the mRNA stability of *PAX6* and *OTX2*, and the loss of IGF2BP2 induces inflammatory and aging phenotypes in RPE cells. *IGF2BP2* knockdown impaired RPE function, leading to retinal dysfunction in vivo.

Conclusions. Our data suggest a crucial role of IGF2BP2 as an m^6A reader in maintaining RPE homeostasis by regulating the stability of *PAX6* and *OTX2*, making it a potential target for preventing the occurrence of retinal diseases related to RPE malfunction.

Keywords: retinal diseases, IGF2BP2, m^6A, PAX6, OTX2, RPE homeostasis

The retinal pigment epithelium (RPE) is a monolayer epithelial cell sheet located in the outermost layer of the retina.[1,2] It serves various important functions, such as light absorption, epithelial transport, secretion of growth factors, participation in the visual cycle, phagocytosis of discarded outer segments of photoreceptors, and establishment of the blood–retinal barrier.[3–5] RPE dysfunction leads to the pathogenesis and progression of retinal diseases, such as age-related macular degeneration (AMD), retinitis pigmentosa, and even vision loss.[6–9]

Extensive research has focused on transcription factors that play indispensable roles in the development and maintenance of RPE cell characteristics.[10–14] D'Alessio et al.[15] previously reported that transduction of foreskin fibroblasts with *PAX6*, *OTX2*, *MITF*, *SIX3*, *GLIS3*, and *FOXD1* could induce cell transformation into RPE, underscoring the significance of these genes in RPE cell differentiation and identity maintenance. PAX6 collaborates with *MITF/TEFC* to ensure proper development of the RPE,[10] and down-regulation of *PAX6* expression decreases melanin pigmentation in the RPE.[16] *OTX2* knockdown leads to a reduction in RPE-specific functions, such as melanogenesis and retinol metabolism, and activates stress signaling pathways and inflammatory genes.[17] *MITF*, a crucial marker gene of

RPE cells, participates in melanin biogenesis and antioxidant stress responses.[18,19] The absence of *MITF* leads to transformation of the RPE into the retina, resulting in degenerative changes in the retina.[19,20]

N^6-methyladenosine (m^6A) mRNA modifications play a critical role in various biological processes[21]. Reversible m^6A methylation is mediated by m^6A modifiers, primarily methyltransferases (METTL3, METTL14, and WTAP), demethylases (FTO and ALKBH5), and readers (YTHDC1/2, YTHDF1/2/3, and IGF2BP1/2/3), which are responsible for recognizing methylated sites.[22,23] m^6A readers are proteins that specifically recognize and bind to the m^6A modification on RNA. Depending on the specific readers recognizing m^6A modifications, m^6A modification serves different biological functions, mainly altering mRNA transcription splicing, enhancing the translation of specific RNAs, or modifying the stability of these RNAs.[23] Mounting evidence suggests the involvement of m^6A modifications and their modulators in AMD pathogenesis.[24–26] However, there is a lack of studies on the regulation of RPE cell characteristics by m^6A modification.

In the current study, we found that insulin-like growth factor 2 mRNA-binding protein 2 (IGF2BP2) regulates RPE homeostasis by recognizing m^6A modifications. IGF2BP2 directly modulates *PAX6* and *OTX2* mRNA stability as an m^6A reader, and IGF2BP2 deficiency attenuates the antioxidant stress response in the RPE, contributing to cellular aging and inflammation. Consistent with in vitro findings, adeno-associated virus (AAV)-sh*IGF2BP2* in the RPE adversely affects visual function, culminating in degenerative changes in the retina in vivo.

Materials and Methods

Clinical Materials

The human eye tissues were obtained from deceased donors who passed away unexpectedly and did not have any known ocular diseases (the health of the eyes was confirmed through examination as the anterior segment tissues were used for transplantation), adhering to the Ethics Committee of the Zhongshan Ophthalmic Center of Sun Yat-Sen University (2023KYPJ231). The research was conducted adhering to the tenets of the Declaration of Helsinki. The donors' information is available in Supplementary Table S1.

Cell Culture

The eye cup was initially immersed in dispase solution and incubated at 37°C for 40 minutes. Subsequently, the retina was dissected from the optic nerve, and the RPE layer was gently separated from the eye cup. The RPE layer was then transferred to 0.05% trypsin–EDTA solution and incubated at 37°C for 10 minutes. Ultimately, RPE cells were seeded onto cell culture dishes precoated with 10% Matrigel and maintained in Dulbecco's modified Eagle's medium (DMEM) supplemented with 10% fetal bovine serum and 1% penicillin/streptomycin.[27] Reagent information is provided in Supplementary Table S1.

Histopathology and Immunofluorescence Staining

RPE and retinal flatmounts were fixed in 4% polyformaldehyde for 15 minutes at room temperature, and mouse eyeballs were fixed with 10% formalin for 3 hours. Subsequently, mouse eyeballs were fixed, dehydrated, embedded in paraffin, sectioned, and stained with hematoxylin and eosin (H&E). For immunofluorescence staining, after paraffin embedding and deparaffinization, tissue sections were subjected to antigen retrieval, followed by permeabilization and blocking using a solution containing 0.3% Triton X-100 and 3% bovine serum albumin. Subsequently, the samples underwent overnight incubation with primary antibodies under conditions maintained at 4°C. The next day, secondary antibodies were incubated for 1 hour. The cell nuclei were counterstained with 4′,6-diamidino-2-phenylindole (DAPI). Antibody information is provided in Supplementary Table S2.

RNA Interference

Two short-hairpin RNAs (shRNAs) targeting *IGF2BP2*, *IGF2BP3*, YTH N^6-methyladenosine RNA binding protein 1 (*YTHDF1*), *YTHDF2*, *YTHDF3*, and *YTHDC1* were cloned into the PLKO.1 lentiviral plasmid. RPE cells underwent transfection with lentiviral particles encoding shRNAs for approximately 24 hours, followed by selection with 1.5- µg/mL puromycin for 48 hours. After drug screening, the cells were passaged once, and the transduction efficiency was ultimately validated by quantitative PCR (qPCR). Scrambled shRNA, which did not target any known gene, was employed as a negative control. The shRNAs employed in our study are provided in Supplementary Table S3.

Phagocytosis Assay

Photoreceptor outer segments (POS) were isolated from porcine eyes and labeled by fluorescein isothiocyanate (FITC) according to a protocol outlined by Parinot et al.[28] Preceding the commencement of the cellular phagocytosis assay, RPE cells were passaged onto 0.4- µm Transwell inserts (3470; Corning, Corning, NY, USA) coated with 10% Matrigel. Before POS were added, primary RPE cells were pretreated with 30% FBS for 1 hour to induce phagocytosis in RPE cells.[29] Then, 10^6 FITC-labeled POS were added to RPE cells and incubated for 1 hour at 37°C. The unbound POS were removed by washing with PBS before fixation. Image J (National Institutes of Health, Bethesda, MD, USA) was used for POS quantification. We applied a double-blinding method to ensure that the experimental results were unbiased.

MitoTracker

Cells were treated with 100-nm/mL MitoTracker Red CMXRos dye (Thermo Fisher Scientific, Waltham, MA, USA), and the incubation was carried out at 37°C for 30 minutes. Post-incubation, the cells were fixed with paraformaldehyde at –20°C for 20 minutes. The specimens were examined under a LSM 800 microscope (ZEISS, Oberkochen, Germany).

Cellular Reactive Oxygen Species Assay

RPE cells were dissociated into single cells using 0.05% trypsin EDTA. After centrifugation and resuspension, 2′,7′-dichlorofluorescin diacetate (DCFDA) dye was added to the cells, followed by an incubation at 37°C for 30 minutes. Subsequently, the cells were analyzed using flow cytometry.

Investigative Ophthalmology & Visual Science

qPCR and RNA Decay Assays

For RNA decay assays, RPE cells were exposed to actinomycin D or dimethyl sulfoxide (DMSO), and total RNA was collected at the 2 and 4 hours post-treatment. Total RNA was isolated from cells using an RNeasy Mini Kit (QIAGEN, Hilden, Germany). We employed the PrimeScript RT Master Mix Kit (Takara Bio, Shiga, Japan) to reverse transcribe RNA into cDNA. qPCR was conducted using the iTaq Universal SYBR Green Supermix Kit (Bio-Rad, Hercules, CA, USA). The housekeeping gene glyceraldehyde-3-phosphate dehydrogenase (GAPDH) was used as a normalization control. A list of the primer used is provided in Supplementary Table S4.

HITS-CLIP Experiment

The high-throughput sequencing of RNA isolated by crosslinking immunoprecipitation (HITS-CLIP) experiment was based on a protocol described by Moore et al.,[30] with slight modifications. Briefly, RPE cells were transfected with lentivirus particles encoding FLAG-IGF2BP2. Cells were ultraviolet crosslinked by irradiation once at 400 mJ cm^2 and then again at 200 mJ cm^2. Cells were then collected and lysed, and cellular RNA was fragmented. Subsequently, the fragmented RNA was incubated with an anti-FLAG antibody, and then antibody–RNA complexes were recovered through immunoprecipitation. After purification by transfer to a nitrocellulose membrane, the antibody–RNA complexes were eluted using proteinase K. The RNA was further purified and subjected to sequencing.

HITS-CLIP Data Analysis

The HITS-CLIP assay was based on a protocol described by Moore et al.[30] The raw reads underwent quality assessment using FASTQC 0.0.2. The HITS-CLIP reads aligned to the hg19 human reference genome by using the Burrows–Wheeler Aligner (BWA) tool. For mutation site identification, crosslink-induced mutation sites (CIMS) software and the Perl tool were utilized to search mutation sites in the BWA alignment and tag sequences, selecting robust CIMS with a false discovery rate (FDR) of $\leq$ 0.001. The nucleotides spanning -10 to $+10$ of the CIMS were obtained in the Browser Extensible Data (BED) file format for subsequent motif analysis. MEME 5.5.5 was used for the de novo motif analysis with $P \leq 0.01$.[31]

RNA-Seq Data Analysis

The raw reads underwent quality assessment using FASTQC 0.11.5[32] and were subsequently trimmed to eliminate adaptor sequences using Trimmomatic 0.39 tools. RNA-seq reads were aligned to the hg19 human reference genome using STAR software,[33] and the calculation of transcripts per million (TPM) values was carried out using the RNA-seq by expectation-maximization (RSEM) tool.[34] Differentially expressed genes were identified using the DESeq2 R package (R Foundation for Statistical Computing, Vienna, Austria). The criteria for selection included a $\log_2$ fold change of $\geq$1 and a FDR of $<$0.05.[35] We employed the online software Metascape (www.metascape.org) for Gene Ontology (GO) enrichment analysis. The parameters were set with cutoffs of $P = 0.01$ and $q = 0.05$.[36]

Animal Model and Treatment

The design and experimental protocols for animal experiments were approved by the Animal Experiment Ethics Committee of Zhongshan Ophthalmic Center, Sun Yat-Sen University (W2023006). C57BL/6 mice (6–8 weeks old, 18–23 g in weight) were purchased from the Guangdong Laboratory Animal Center (Guangzhou, China) and maintained in the animal facility of the Zhongshan Ophthalmic Center at Sun Yat-Sen University (Guangzhou, China). Mice were housed under a 12-hour light/dark cycle and fed ad libitum. After anesthesia, 1 µL CNV-ZSGREEN-AAV2-U6-sh*IGF2BP2* (10^{11} viral particles/µL) was injected into the subretinal space, and the paired eye was injected with negative control AAV.

Optical Coherence Tomography Evaluation

An intraperitoneal injection of 0.6% pentobarbital sodium was administered for mouse anesthesia (100 µL/10 g). Pupils were dilated using tropicamide ophthalmic drops, and corneas were lubricated with hypromellose gel. Optical coherence tomography (OCT; Heidelberg Engineering, Heidelberg, Germany) was performed on both eyes to investigate structural changes. Heidelberg Eye Explorer software was used to compute retinal thickness and volume.

Electroretinography Testing

Prior to the electroretinography (ERG) test, recorded using a Celeris rodent ERG device (Diagnosys, Lowell, MA, USA), mice underwent overnight dark adaptation. After the mice were anesthetized, pupil dilation was performed, and the surface of the eyes was kept moist. Electrodes were positioned atop each cornea, and scotopic and photopic ERG responses were subsequently recorded. The light-adapted ERG was conducted subsequent to dark-adapted ERG. Following a 10-minute light adaptation (30 cd/m^2; white, 6500K), photopic ERG was executed with flash intensities ranging from 0.3 to 30 cd s/m^2. The C-waves followed a 100-ms light stimulus (150 cd/m^2; white, 6500K).

Western Blot Analysis

The RPE–choroid tissues, retina, and RPE cells were lysed in 100 µL radioimmunoprecipitation assay (RIPA) buffer and supplemented with protease inhibitor cocktails and protein phosphatase inhibitors. Tissues were also sonicated. For the western blotting analysis, 20 to 50 µg of total protein was used.

Statistical Analysis

Prism 6 (GraphPad, Boston, MA, USA) was used for the statistical analyses. The unpaired two-tailed Student's *t*-test was used to determine the significance of differences between groups. For multiple condition comparisons, Šídák's multiple comparisons test was used. Data are presented as means $\pm$ SD. Details on replicates performed for each experiment can be found in the figure legends.

Results

IGF2BP2 Modulates RPE Phagocytosis

Phagocytosis is a major physiological function of the RPE[37]; therefore, phagocytic ability was used as an observational parameter to investigate the effects of m^{6}A regulation on RPE cells. Primary cultured RPE cells were characterized by positive staining for RPE65, PAX6, MITF, OTX2, and ZO-1 (Supplementary Fig. S1A). m^{6}A-related reader genes, including *IGF2BP2*, *IGF2BP3*, *YTHDC1*, *YTHDF1*, *YTHDF2*, and *YTHDF3*, were knocked down by shRNA transfection (Supplementary Fig. S1B). The phagocytic function was assessed using the experimental scheme outlined in Figure 1A.[29] *Z*-stack fluorescence imaging revealed the intracellular localization of fluorescence-labeled POS, confirming the phagocytic capability of ex vivo cultured RPE cells (Fig. 1B). We found that IGF2BP2 was the most effective m^{6}A reader affecting RPE phagocytosis among the candidates, with the number of phagocytosed POS being only 56.6% of those in the control group (Figs. 1B, 1C), suggesting that IGF2BP2 is a principal m^{6}A-related player in the regulation of RPE cell function.

IGF2BP2 Affects Cellular Function by Regulating the mRNA Stability of *PAX6* and *OTX2*

To further gain insight into the influence of IGF2BP2 on the RPE, we compared the transcriptional profiles of *IGF2BP2* knocked-down RPE cells (sh*IGF2BP2*-RPE group) with those of control RPE cells (Supplementary Fig. S1B). Principal component analysis indicated that the excellent intragroup sample reproducibility and gene expression pattern in the sh*IGF2BP2*-RPE group were quite distinct from those in the control group (Supplementary Fig. S2A). A total of 786 and 472 mRNAs were downregulated and upregulated, respectively, in the sh*IGF2BP2*-RPE group. Notably, the loss of IGF2BP2 resulted in the downregulation of crucial genes that maintain the characteristics of the RPE, such as *MITF*, *PAX6*, and *OTX2*. Moreover, the expression of a series of genes that are linked to the biological processes of the retinoid cycle (*RARRES2*, *RBP1*, *CRABP2*), secretion (*SERPINF1*), phagocytosis (*MYO7A*, *GULP1*, *RAP1GAP*), and pigmentation (*MYO7A*, *SPNS2*) (Fig. 2A) were decreased in the sh*IGF2BP2*-RPE group. Consistent results were obtained using GO and Gene Set Enrichment Analysis (GSEA) analyses (Fig. 2B, Supplementary Fig. S2B).[38]

IGF2BP2, an m^{6}A reader, was previously reported to enhance RNA stability by recognizing m^{6}A modifications in RNA.[22,23] To gain a deeper understanding of how IGF2BP2 affects the expression of characteristic genes in RPE cells, HITS-CLIP assays were performed.[30] The HITS-CLIP results identified IGF2BP2-binding RNAs and their specific binding sites. Among the CIMS, 41.7% were found to be distributed across the 5′ untranslated regions (UTR), coding sequences (CDSs), and 3′ UTR (Fig. 2C). Most sites were concentrated around the start and stop codons, as well as the 3′ UTR (Fig. 2D). m^{6}A is a co-transcriptional modification that occurs in the sequence context RRACH (R = A or G; H = A, C, or U; A = m^{6}A).[39] Motif enrichment analysis of the m^{6}A-containing peaks was performed using CIMS, which revealed three distinct consensus motifs centered on the AC core of the m^{6}A motif, which was significantly enriched (Fig. 2E). A total of 5335 RNAs associated with these three motifs intersected with genes that were downregulated in the sh*IGF2BP2*-RPE group, and 180 overlapping genes were identified (Fig. 2F). GO analysis of these genes revealed a decline in cell fate specification, pigmentation, secretion by cells, and response to retinoic acid (Fig. 2G). Analysis of the HITS-CLIP assay results revealed m^{6}A modifications at the sites where IGF2BP2 binds to *OTX2* and *PAX6* (Fig. 2H). Treatment of RPE cells with the METTL3 inhibitor STM2457[40] led to decreased stability of *OTX2* and *PAX6* (Fig. 2I), suggesting regulation of *PAX6* and *OTX2* mRNA stability by m6A modification. Moreover, inhibition of IGF2BP2 binding to m^{6}A modification sites using CWI1-2[41] resulted in a notable reduction in *PAX6* and *OTX2* expression levels (Supplementary Fig. S2C). RNA decay assays further demonstrated that *IGF2BP2* knockdown significantly diminished the stability of *PAX6* and *OTX2* mRNA in RPE cells (Fig. 2J), highlighting the recognition of m6A modifications on mRNA by IGF2BP2, thereby modulating their stability. Moreover, we observed that the downregulation of IGF2BP2 and PAX6 expression was accompanied by a decrease in MITF expression (Figs. 2K, 2L). Therefore, we propose that IGF2BP2 influences these regulatory networks by affecting the functionality and homeostasis of RPE cells, thereby ensuring proper physiological function through the recognition and stabilization of essential transcription factors.

Knockdown of *IGF2BP2* Induces Senescence of RPE Cells

Notably, 5-ethynyl-2′-deoxyuridine (EdU) staining of cells indicated a decrease in cell proliferation after *IGF2BP2* knockdown (Supplementary Figs. S3A, S3B). Meanwhile, RNA-seq data revealed that the upregulated genes following *IGF2BP2* knockdown are enriched in cellular aging, suggesting a permanent cell-cycle arrest in RPE cells (Fig. 3A, Supplementary Figs. S3C, S3D). Beta-galactosidase staining indicated a significant increase in the proportion of senescent cells in the *IGF2BP2* knockdown group (Figs. 3B, 3C). Strikingly, cellular reactive oxygen species (ROS) levels were elevated in the sh*IGF2P2*-RPE cells (Fig. 3D), and downregulation of IGF2BP2 expression led to mitochondrial fission, which indicated low mitochondrial membrane potential (MMP) (Fig. 3E).[42] Reduced MMP suggests potential damage to the mitochondria, which implies the release of more cellular ROS. Thus, these results indicate that *IGF2BP2* knockdown led to cellular oxidative stress and triggered senescence.

IGF2BP2 Deficiency Impairs RPE Function

To explore the in vivo regulatory role of IGF2BP2 in the RPE, we initially verified the expression of IGF2BP2 in RPE–choroid tissues using immunofluorescence staining (Fig. 4A). We then used an AAV containing the sh*IGF2BP2* sequence with a ZSGREEN reporter to suppress IGF2BP2 expression in mouse RPE by subretinal injection (Fig. 4B, Supplementary Fig. S4A). Using whole-mount ZSGREEN imaging of RPE cells, we observed the successful transfection of RPE cells (Supplementary Fig. S4B). In comparison with the control group, the AAV-shIGF2BP2–infected group exhibited a substantial reduction in IGF2BP2 mRNA and protein levels in the RPE (Fig. 4C, Supplementary Fig. S4C), whereas IGF2BP2 expression in the retinal layers did not change (Supplementary Fig. S4D).

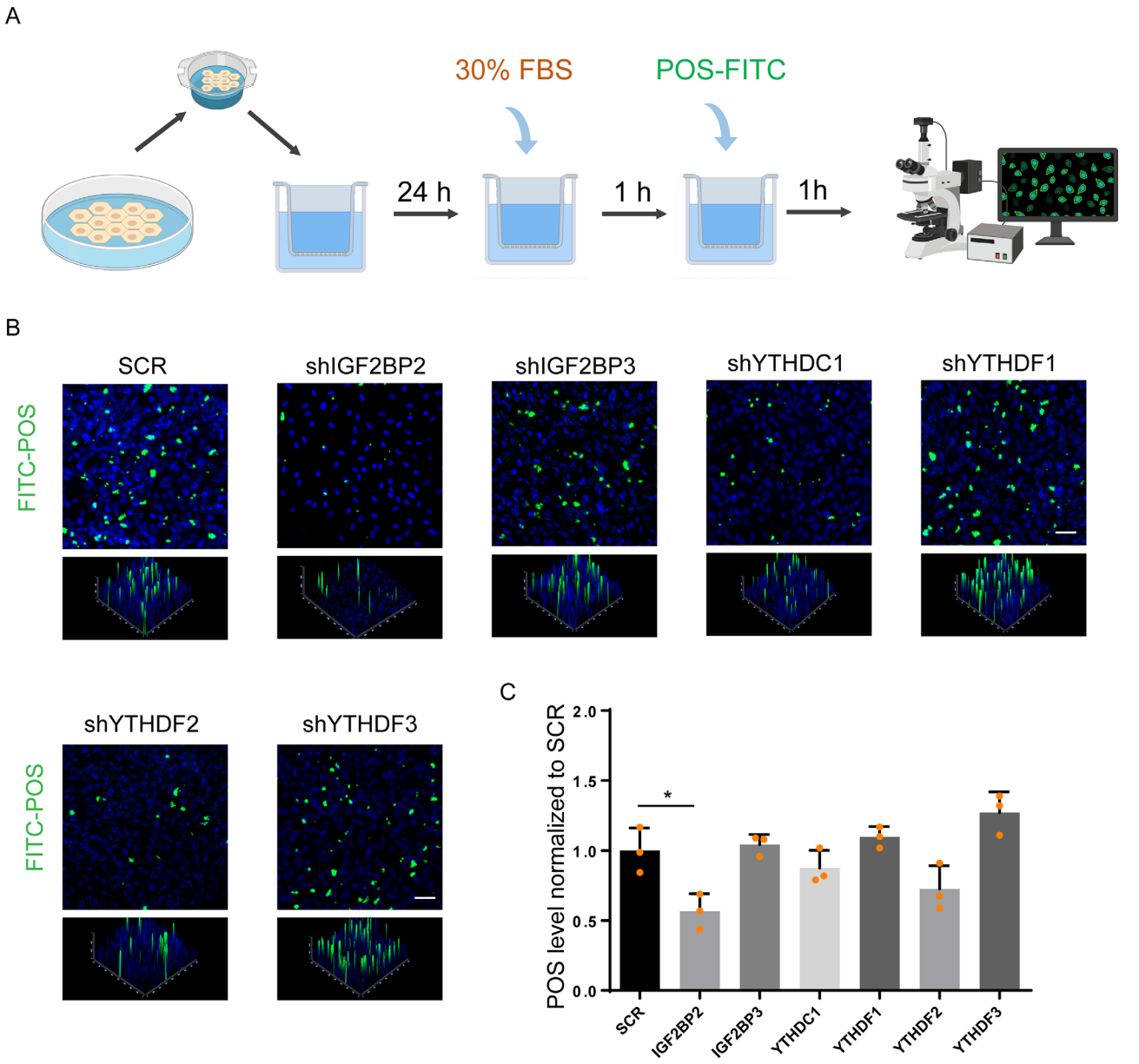

Figure 1. IGF2BP2 controlled RPE phagocytosis. (**A**) Experimental scheme for detecting the phagocytic function of RPE cells. (**B**) FITC-labeled POS were visualized in RPE cells transduced with scrambled shRNA-(SCR), sh*IGF2BP2*, sh*IGF2BP3*, sh*YTHDC1*, sh*YTHDF1*, sh*YTHDF2*, and sh*YTHDF3* ($n = 3$ biological replicates). *Scale bar*: 50 µm. (**C**) Quantification of POS in RPE cells for the indicated transfection. For each group, five regions were randomly selected. *$P < 0.05$ (two-tailed unpaired *t*-test; $n = 3$ for each group).

Subsequently, the F-actin dye phalloidin was used to assess RPE morphology in flatmounted retinal tissues at 10 days post-virus injection. Compared to the RPE layer of the control group, which exhibited a regular hexagonal configuration, there was a notable increase in cell size and aberrant cell morphology in the sh*IGF2BP2*-RPE group (Fig. 4D). Functional tests of RPE phagocytosis revealed that ex vivo RPE in the knockdown group showed decreased adherence to the outer segments of photoreceptors compared with that in the control group in the morning (9:00 AM). There was an increase in intracellular and extracellular outer segments (labeled with opsin) over time in the shIGF2BP2 group, whereas the control group showed a decrease in outer segments over time (Fig. 4E). These results suggest a diminished ability of the RPE in the knockdown group to phagocytose and digest photoreceptor outer segments.

Consistent with previous findings in vitro, fluorescence staining and quantitative qPCR showed that knockdown of *IGF2BP2* led to downregulation of RPE65, PAX6, MITF, and OTX2 expression in the sh*IGF2BP2*-RPE group of mice (Figs. 4F, 4G). Moreover, mRNA expression of *RBP1*, *LRAT*, *RDH5*, *TYR*, *MYO7A*, *GULP1*, and *APPL2*, which encode essential RPE-specific proteins involved in the visual cycle, pigmentation, and phagocytosis, was also reduced in the AAV-sh*IGF2BP2*-RPE group (Fig. 4G). These data suggest a pivotal role for IGF2BP2 in maintaining the function and characteristics of RPE cells.

Investigative Ophthalmology & Visual Science

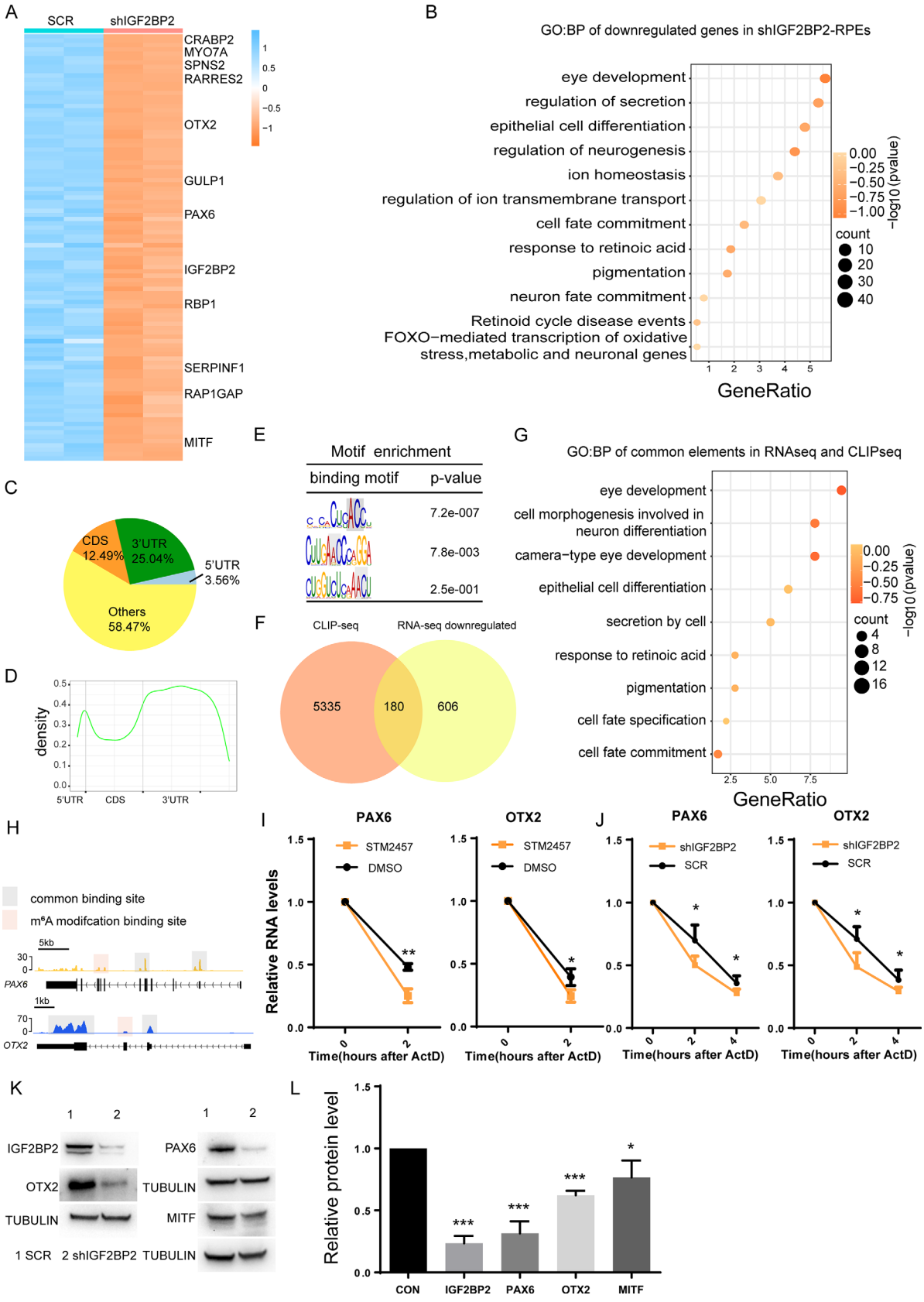

Figure 2. Gene regulatory network analysis identified IGF2BP2 controlling RPE cell characteristics. (**A**) Heatmap demonstrated normalized transcripts per million reads (TPM) values of the top 100 downregulated genes in the sh*IGF2BP2*-RPE group, with the addition of the gene list of Supplementary Table S5. (**B**) GO analysis of downregulated genes in the sh*IGF2BP2*-RPE group. (**C**) Pie charts depicting the proportions of peak distributions in the 5′ UTR, CDS, and 3′ UTR regions across the CIMS. (**D**) Metagene profiles of CIMS distribution across the 5′ UTR, CDS, and 3′ UTR regions in RPE cells. (**E**) Each sequence motif was identified within m^{6}A peaks by MEME analysis of the CIMS.

Investigative Ophthalmology & Visual Science

(**F**) Venn diagram indicates the overlapping and unique genes for the CIMS containing the m^{6}A peak and RNA-seq downregulated genes. (**G**) GO analysis of the common elements between the CIMS containing the m^{6}A peak and RNA-seq downregulated genes. (**H**) Genome browser tracks for the indicated CIMS and m^{6}A peak signals across the *PAX6* and *OTX2* loci. (**I**) Representative mRNA profile of *PAX6* and *OTX2* at indicated time points after actinomycin D (ActD) treatment (5 µg/mL) in RPE cells treated by DMSO and STM2457 for 24 hours (10 µm). The qPCR values were normalized to the values in the cells for the 0-hour time point. $^*P < 0.05$ (two-tailed unpaired *t*-test; $n = 3$ for each group). (**J**) Representative mRNA profile of *PAX6* and *OTX2* at indicated time points after ActD treatment (5 µg/mL) in the scrambled shRNA-(SCR) and sh*IGF2BP2*-RPE groups. The qPCR values were normalized to the values in the cells for the 0-hour time point. $^*P < 0.05$, $^{**}P < 0.01$ (two-tailed unpaired *t*-test; $n = 5$ for each group). (**K**) Western blot analysis of IGF2BP2, PAX6, OTX2, and MITF protein levels with the indicated treatments. (**L**) Quantification of western blot analysis; values were normalized to the values in the control cells. $^*P < 0.05$, $^{***}P < 0.001$ (two-tailed unpaired *t*-test; $n = 3$ for each group).

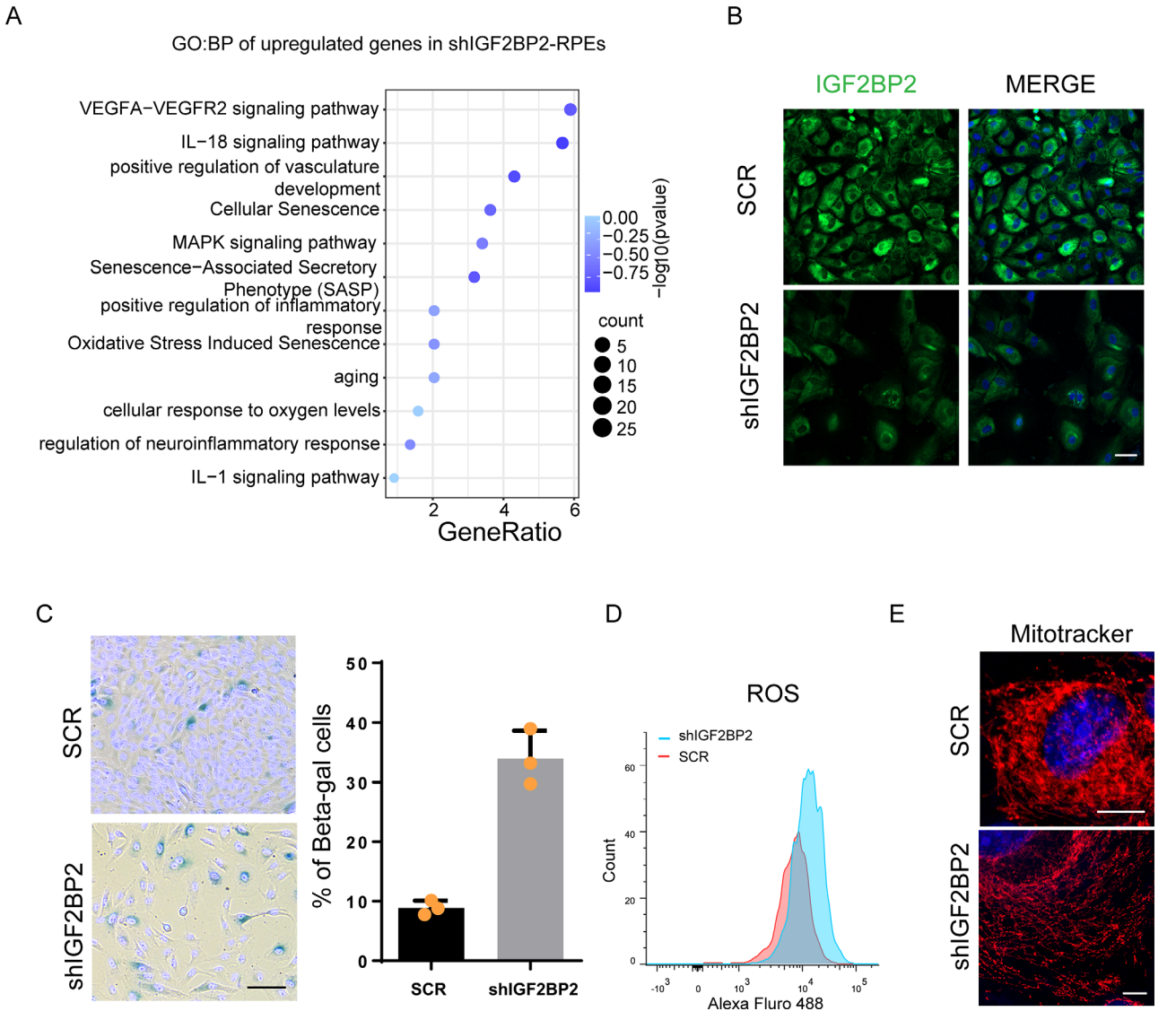

Figure 3. Knockdown of *IGF2BP2* induced cellular senescence. (**A**) GO analysis of upregulation genes in the sh*IGF2BP2*-RPE group. (**B**) Image of RPE cells stained with IGF2BP2 ($n = 3$). *Scale bar*: 50 µm. (**C**) Quantification of beta-galactosidase–positive RPE cells for the indicated transfections. For each group, five regions were randomly selected. $^{**}P < 0.01$ (two-tailed unpaired *t*-test; $n = 3$ for each group). (**D**) ROS production levels in the control group and sh*IGF2BP2*-RPE group measured by flow cytometry ($n = 3$). (**E**) MitoTracker fluorescence was detected in the control and sh*IGF2BP2*-RPE groups ($n = 3$). *Scale bar*: 10 µm.

Knockdown of *IGF2BP2* Affects Visual Function In Vivo

The RPE is critical for maintaining retinal homeostasis, and retinal photoreceptor cells tend to degenerate or even die when RPE function declines, ultimately resulting in retinal atrophy.[43,44] To elucidate visual dysfunction in response to IGF2BP2 suppression, sh*IGF2BP2* mice were subjected to ERG measurements 1, 2, and 4 weeks after AAV injection. The C-wave was significantly reduced at each time

Investigative Ophthalmology & Visual Science

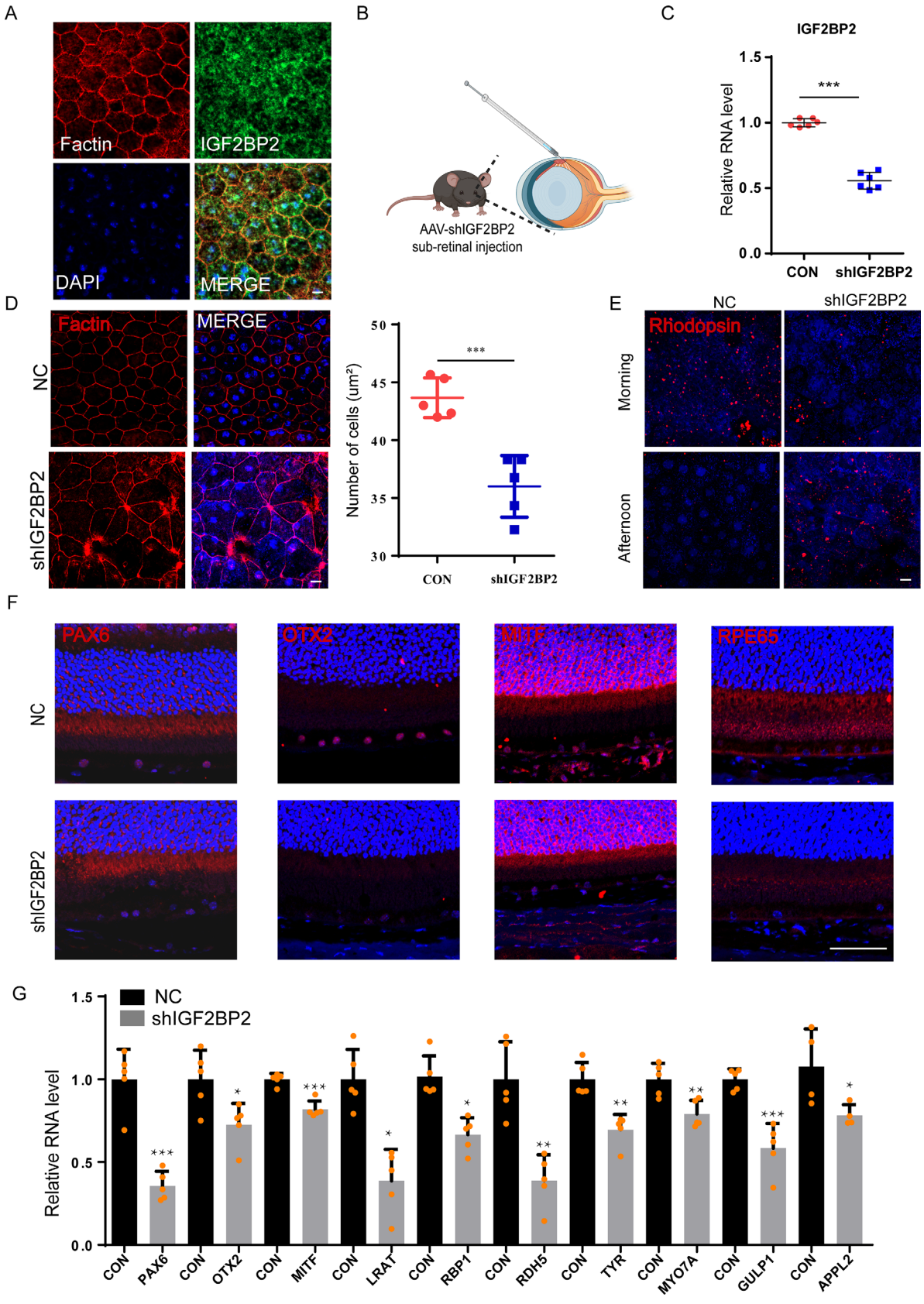

Figure 4. Knockdown of IGF2BP2 affected mice RPE identity. (**A**) Fluorescence image of IGF2BP2 and F-actin in RPE–choroid tissues. *Scale bar*: 10 µm. (**B**) Animal experimental scheme. Negative control (NC) AAV or AAV-shIGF2BP2 was delivered into the subretinal space of 6- to 8-week-old mice. (**C**) qPCR shows mRNA expression of RPE cells at 10 days after injection. ***$P < 0.001$ (two-tailed unpaired *t*-test; $n = 6$ mice). (**D**) Quantification of cell number from F-actin fluorescence image at 10 days. ***$P < 0.001$ (two-tailed unpaired *t*-test; $n = 5$ mice). *Scale bar*: 10 µm. (**E**) Rhodopsin fluorescence was detected as an indicator of phagocytic function of RPE cells in the morning (9:00

Investigative Ophthalmology & Visual Science

AM) and afternoon (4:30 PM) at 10 days after injection ($n = 3$ mice). *Scale bar*: 10 µm. (**F**) Immunostaining image of PAX6, OTX2, MITF, and RPE65 in the posterior eye segments after injection for 10 days ($n = 3$ mice). *Scale bar*: 50 µm. (**G**) qPCR presenting mRNA expression of RPE cells at 10 days after injection. qPCR values were normalized to the values in control cells. The genes validated by qPCR were selected based on their differential expression from RNA-seq data following the knockdown of IGF2BP2 in cultured RPE cells.*$P < 0.05$, **$P < 0.01$, ***$P < 0.001$ (two-tailed unpaired *t*-test; $n = 4$ or 5 mice).

point, indicating impaired RPE function.[45] Notably, the C-wave in mice RPE with *IGF2BP2* knockdown exhibited a significant decrease over time (Figs. 5A, 5B). Scotopic ERG responses also significantly declined over time in sh*IGF2BP2* mice, indicating impaired photoreceptor phototransduction (A-wave) and rod bipolar cell depolarization (B-wave) (Figs. 5C–5E).

OCT was used to observe changes in retinal structure. The retina in mice injected with AAV-sh*IGF2BP2* showed progressive thinning over time (Figs. 6A–6C). This finding was corroborated by quantitative topographic volume assessment (Fig. 6D, Supplementary Fig. S5A). H&E staining of the posterior eye segment showed obvious RPE disruption, aberrant photoreceptor morphology, and retinal thinning at 4 weeks after AAV-shIGF2BP2 injection (Fig. 6B). Additionally, because vascular invasion from the choriocapillaris is a crucial indicator of retinal damage, we performed CD18/ITGB2 (IB4) staining in our mouse model. The results revealed the presence of vascular infiltration within the RPE–choroid complex in the *IGF2BP2* knockdown group of mice, which was absent in the control group of mice (Fig. 6E). With the disruption of RPE cell organization and vascular invasion, immunofluorescent staining of Rhodopsin revealed a reduction in photoreceptor cells (indicated by white arrows) (Fig. 6F), and terminal deoxynucleotidyl transferase dUTP nick end labeling (TUNEL) staining demonstrated apoptosis of photoreceptor cells in the *IGF2BP2* knockdown group (Fig. 6G). Taken together, these results reveal that IGF2BP2 plays a crucial role in maintaining retinal visual function and that the knockdown of *IGF2BP2* induces aberrant photoreceptor morphology, retinal thickness thinning, RPE disruption, and photoreceptor cell death. This sequence of events culminates in disturbed retinal homeostasis.

Discussion

Accumulating evidence supports a significant role for m^{6}A modifications in the maintenance of cellular and tissue functions.[23,46,47] Indeed, some readers can enhance RNA stabilization through various mechanisms. Once bound, these proteins may enhance translation, thereby protecting mRNA from degradation; recruit stabilizing proteins that directly prevent decay; or influence mRNA export and localization, ensuring its availability for translation.[21,23] These mechanisms collectively support the longevity and functionality of mRNA within cells. For example, IGF2BP2 recognizes and binds RNA molecules bearing m^{6}A modifications through its K homology (KH) domains.[41,48] Our work emphasizes that IGF2BP2 may function as a reader recognizing m^{6}A modification sites on *PAX6* and *OTX2* mRNA. Decreased levels of IGF2BP2 in RPE cells directly or indirectly lead to decreased expression of PAX6, OTX2, and MITF, thereby impacting various functions of RPE cells such as visual circulation and phagocytosis. This disruption ultimately compromises the ability of the retina to maintain its homeostasis and suggests its potential as a target for preventing the occurrence of retinal disease related to RPE malfunction.

In the in vitro culture of RPE cells, cell density can influence cell polarity, thereby affecting cell function.[4,49] In this study, we found that knockdown *IGF2BP2* led to a decrease in the expression of important transcription factors in RPE cells, such as PAX6, OTX2, and MITF, resulting in slower cell proliferation and cell aging. Consequently, the decrease in cell density affected cell polarity and differentiation, partially impacting cell function. This interplay likely represents one of the mechanisms through which *IGF2BP2* knockdown affects RPE cell function. Future studies will further investigate the specific effects of *IGF2BP2* knockdown on RPE cell polarity and function. RPE dysfunction plays a crucial role in the pathogenesis and progression of retinal diseases.[7,43,50] A reduction in the RPE phagocytic, secretory, and visual cycle is associated with the occurrence of retinal degenerative diseases, such as AMD, retinitis pigmentosa, and Stargardt disease.[4,51–53] Impairment of the RPE barrier function can lead to pathologies such as AMD and macular edema.[4,54] Our in vivo mouse study involving *IGF2BP2* knockdown in the RPE showed retinal degeneration, pigment deposition, and choroidal vascular invasion, which align with the characteristic features of AMD. Additionally, knockdown of *IGF2BP2* in RPE cells resulted in upregulation of the AMD-associated gene *THBS1* and inflammatory factors *IL6*, *IGFBP3*, and *ICAM1*.[55,56] A limitation in our study is that the RNA-seq and CLIP-seq samples were derived from donors of different ages. Consequently, this age discrepancy might introduce variability in interpreting the data. Conducting RNA-seq and CLIP-seq on cross-age paired samples could mitigate this limitation. This finding underscores the critical role of IGF2BP2 in maintaining RPE homeostasis and suggests the need for further exploration of its role in retinal diseases.

Research into the m^{6}A readers, including the YTHDF family and YTHDC2, highlights their diverse and significant impacts on eye-related pathologies and RNA dynamics.[26] YTHDF2 has been implicated in RNA degradation and is associated with the regulation of corneal neovascularization.[26,57] YTHDF1/3 has been suggested to play a role in enhanced translation, and YTHDF1, specifically, may play a role in ocular melanoma and oxygen-induced retinopathy.[58,59] YTHDC1 is primarily involved in regulating pre-mRNA splicing and facilitating mRNA nuclear transport, whereas YTHDC2 contributes to mRNA stability and translation.[21,23] Elevated expression of YTHDF2 and YTHDC2 in the serum of patients with Graves' ophthalmopathy suggests the potential involvement of m^{6}A modifications in secondary eye diseases.[60] HNRNPC/G and HNRNPA2B1 indirectly bind to transcripts that have undergone alternative splicing or processing that results in structural transformations, whereas IGF2BP family readers (IGF2BP1/2/3) primarily enhance mRNA stability and promote mRNA translation.[22,23,61] Currently, there is a paucity of information regarding the regulatory roles of HNRNPC/G, HNRNPA2B1, and IGF2BP1/2/3 in normal and diseased eye tissues. Our study sheds light on the pivotal role of IGF2BP2 in maintaining the normal physiological state of RPE cells and shows that

Investigative Ophthalmology & Visual Science

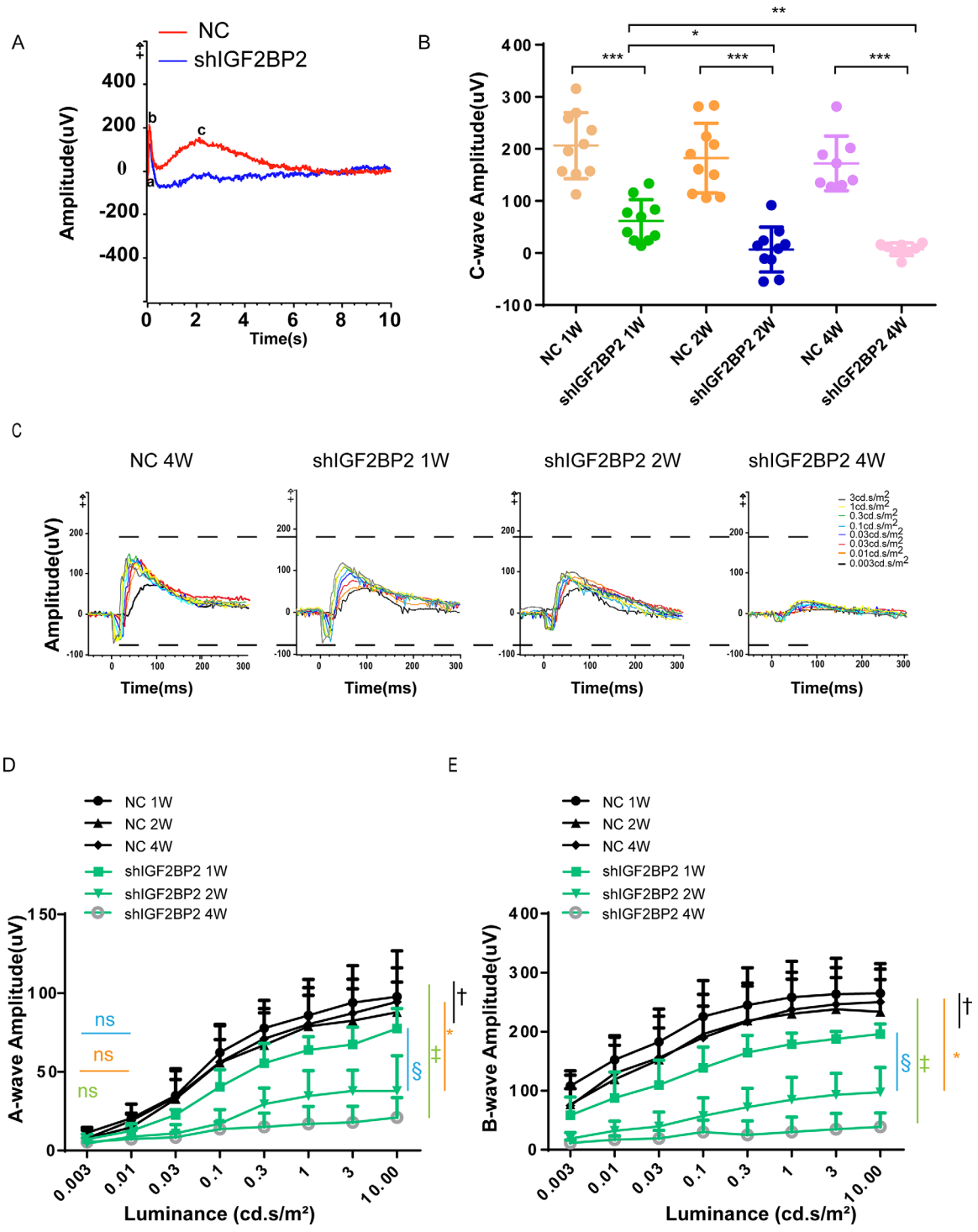

Figure 5. Knockdown of *IGF2BP2* diminished electrical activity of the mice retina. (**A**) ERG-recorded C-waves at 2 weeks after AAV vector injection. (**B**) Quantification of C-wave ERG amplitude following a 100-ms light stimulus (150 cd/m^2; white, 6500K). *$P < 0.05$, **$P < 0.01$, ***$P < 0.001$ (unpaired two-tailed Student's *t*-test; $n = 10$ mice 1 and 2 weeks old and $n = 6$ mice 4 weeks old). (**C**) ERG-recorded scotopic A-waves and B-waves at 1, 2, and 4 weeks after injection. (**D**) Quantification of A-wave ERG amplitudes. ns, not significant; *, †, ‡, and § symbols indicate statistical significance determined using the Holm–Šídák method, with alpha = 5.000% (multiple *t*-tests; $n = 6$ mice 1 week old, $n = 8$ mice 2 weeks old, and $n = 8$ mice 4 weeks old). *Black line* indicates 1-week-old NC versus 1-week-old sh*IGF2BP2*; *orange line* indicates 2-week-old NC versus 2-week-old sh*IGF2BP2*; *green line* indicates 4-week-old NC versus 4-week-old sh*IGF2BP2*; *blue line* indicates 1-week-old sh*IGF2BP2* versus 2-week-old sh*IGF2BP2*. (**E**) Quantification of B-wave ERG amplitudes. ns, not significant; *, †, ‡, and § symbols indicate statistical significance determined using the Holm–Šídák method, with alpha = 5.000% (multiple *t*-test; $n = 6$ mice 1 week old, $n = 8$ mice 2 and 4 weeks old). *Black line* indicates 1-week-old NC versus 1-week-old sh*IGF2BP2*; *orange line* indicates 2-week-old NC versus 2-week-old sh*IGF2BP2*; *green line* indicates 4-week-old NC versus 4-week-old sh*IGF2BP2*; *blue line* indicates 1-week-old sh*IGF2BP2* versus 2-week-old sh*IGF2BP2*.

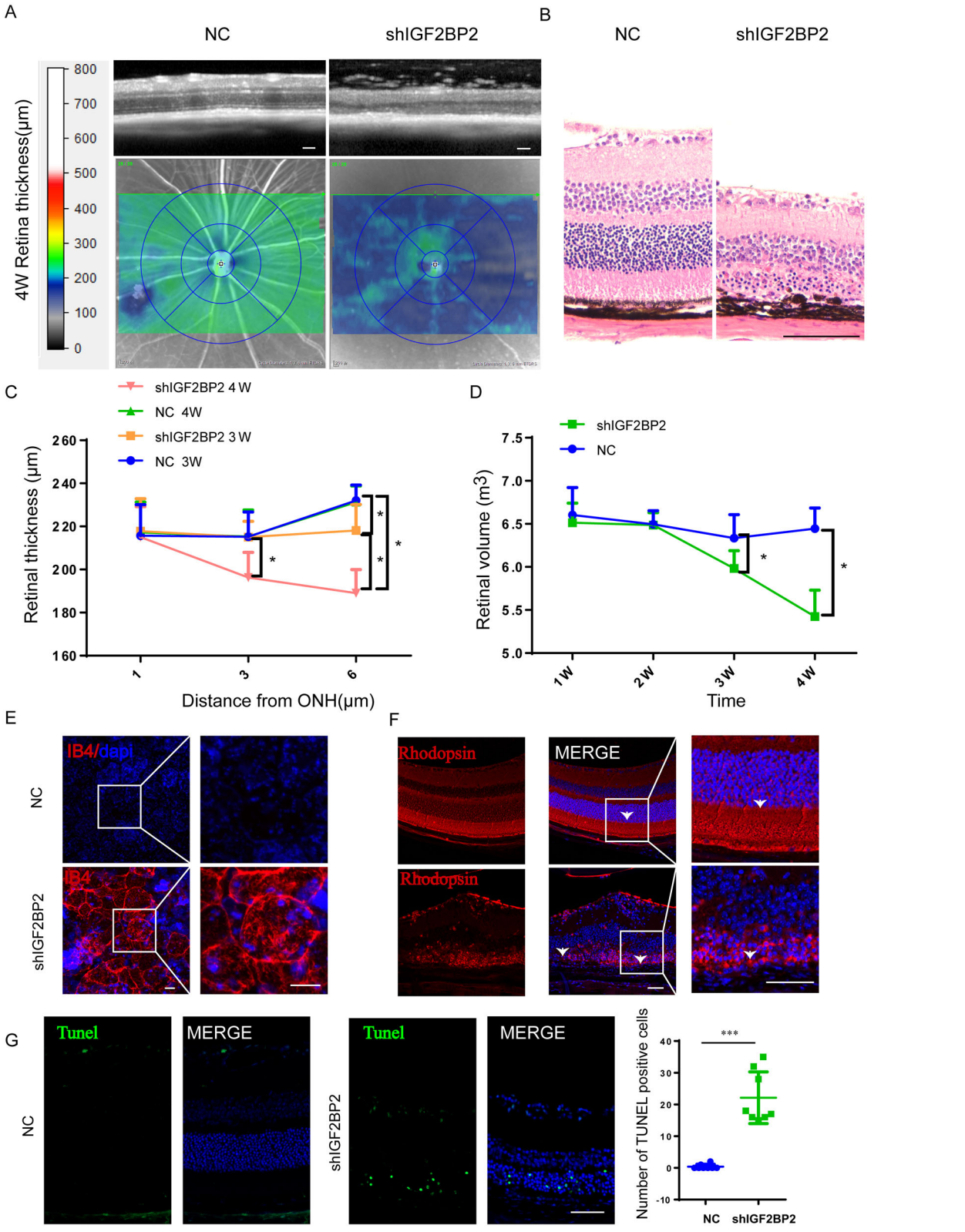

Figure 6. Knockdown of *IGF2BP2* disrupts mice retina homeostasis. (**A**) OCT scan of mice at 4 weeks. *Scale bar*: 200 µm. (**B**) H&E staining of the posterior eye segments after injection for 30 days ($n = 5$ per group). *Scale bar*: 100 µm. (**C**) Quantification of retinal thickness of OCT at 3 and 4 weeks. ns, not significant; asterisk (*) indicates statistical significance determined using the Holm–Šídák method, with alpha = 5.000% (multiple *t*-test; $n = 10$ mice). (**D**) Quantification of retinal volume of OCT at 1 to 4 weeks. ns, not significant; asterisk (*) indicates statistical significance determined using the Holm–Šídák method, with alpha = 5.000% (multiple *t*-test; $n = 10$ mice). (**E**) Fluorescence image

Investigative Ophthalmology & Visual Science

of IB4 in RPE–choroid tissues (n = 5 mice). *Scale bar*: 10 µm. (**F**) Rhodopsin was detected in the posterior eye segments after injection for 30 days (n = 5 mice). *Scale bar*: 50 µm. (**G**) Quantification of TUNEL-positive cell number in posterior eye sections. *Scale bar*: 50 µm. ***$P < 0.001$ (two-tailed unpaired t-test; n = 5 mice, for each of which one or two regions were randomly selected).

IGF2BP2 knockdown can lead to retinal dysfunction in vivo.

Acknowledgments

Supported by grants from the National Natural Science Foundation of China (82371082), Guangzhou Science and Technology Program (2024A03J0254/SL2024A03J00493), Young Teacher Training Program of Sun Yat-Sen University (09667-12230012), and Guangdong Basic and Applied Basic Research Foundation (2021A1515010468).

Disclosure: **S. Wu**, None; **F. Li**, None; **K. Mo**, None; **H. Huang**, None; **Y. Yu**, None; **Y. Huang**, None; **J. Liu**, None; **M. Li**, None; **J. Tan**, None; **Z. Lin**, None; **Z. Han**, None; **L. Wang**, None; **H. Ouyang**, None

References

1. Blair K, Czyz CN. Retinal detachment. In *StatPearls [Internet]*. Treasure Island, FL: StatPearls Publishing; 2024.
2. Bok D. The retinal pigment epithelium: a versatile partner in vision. *J Cell Sci Suppl*. 1993;17:189–195.
3. Lakkaraju A, Umapathy A, Tan LX, et al. The cell biology of the retinal pigment epithelium. *Prog Retin Eye Res*. 2020;78:100846.
4. Strauss O. The retinal pigment epithelium in visual function. *Physiol Rev*. 2005;85:845–881.
5. Benedicto I, Lehmann GL, Ginsberg M, et al. Concerted regulation of retinal pigment epithelium basement membrane and barrier function by angiocrine factors. *Nat Commun*. 2017;8:15374.
6. Chakravarthy U, Peto T. Current perspective on age-related macular degeneration. *JAMA*. 2020;324:794–795.
7. Apte RS. Age-related macular degeneration. *N Engl J Med*. 2021;385:539–547.
8. Mercau ME, Akalu YT, Mazzoni F, et al. Inflammation of the retinal pigment epithelium drives early-onset photoreceptor degeneration in Mertk-associated retinitis pigmentosa. *Sci Adv*. 2023;9:eade9459.
9. Tsang SH, Sharma T. Retinitis pigmentosa (non-syndromic). *Adv Exp Med Biol*. 2018;1085:125–130.
10. Bharti K, Gasper M, Ou J, et al. A regulatory loop involving PAX6, MITF, and WNT signaling controls retinal pigment epithelium development. *PLoS Genet*. 2012;8:e1002757.
11. Cohen-Tayar Y, Cohen H, Mitiagin Y, et al. Pax6 regulation of *Sox9* in the mouse retinal pigmented epithelium controls its timely differentiation and choroid vasculature development. *Development*. 2018;145:dev163691.
12. Diacou R, Nandigrami P, Fiser A, Liu W, Ashery-Padan R, Cvekl A. Cell fate decisions, transcription factors and signaling during early retinal development. *Prog Retin Eye Res*. 2022;91:101093.
13. Martinez-Morales JR, Rodrigo I, Bovolenta P. Eye development: a view from the retina pigmented epithelium. *Bioessays*. 2004;26:766–777.
14. Beby F, Lamonerie T. The homeobox gene *Otx2* in development and disease. *Exp Eye Res*. 2013;111:9–16.
15. D'Alessio AC, Fan ZP, Wert KJ, et al. A systematic approach to identify candidate transcription factors that control cell identity. *Stem Cell Reports*. 2015;5:763–775.
16. Raviv S, Bharti K, Rencus-Lazar S, et al. PAX6 regulates melanogenesis in the retinal pigmented epithelium through feed-forward regulatory interactions with MITF. *PLoS Genet*. 2014;10:e1004360.
17. Housset M, Samuel A, Ettaiche M, et al. Loss of Otx2 in the adult retina disrupts retinal pigment epithelium function, causing photoreceptor degeneration. *J Neurosci*. 2013;33:9890–9904.
18. Han S, Chen J, Hua J, et al. MITF protects against oxidative damage-induced retinal degeneration by regulating the NRF2 pathway in the retinal pigment epithelium. *Redox Biol*. 2020;34:101537.
19. Ma X, Li H, Chen Y, et al. The transcription factor MITF in RPE function and dysfunction. *Prog Retin Eye Res*. 2019;73:100766.
20. Ou J, Bharti K, Nodari A, Bertuzzi S, Arnheiter H. *Vax1/2* genes counteract *Mitf*-induced respecification of the retinal pigment epithelium. *PLoS One*. 2013;8:e59247.
21. Zhao BS, Roundtree IA, He C. Post-transcriptional gene regulation by mRNA modifications. *Nat Rev Mol Cell Biol*. 2017;18:31–42.
22. Meyer KD, Jaffrey SR. The dynamic epitranscriptome: N^6-methyladenosine and gene expression control. *Nat Rev Mol Cell Biol*. 2014;15:313–326.
23. Shi H, Wei J, He C. Where, when, and how: context-dependent functions of RNA methylation writers, readers, and erasers. *Mol Cell*. 2019;74:640–650.
24. Chen X, Wang Y, Wang JN, et al. m^6A modification of circSPECC1 suppresses RPE oxidative damage and maintains retinal homeostasis. *Cell Rep*. 2022;41:111671.
25. Sun RX, Zhu HJ, Zhang YR, et al. ALKBH5 causes retinal pigment epithelium anomalies and choroidal neovascularization in age-related macular degeneration via the AKT/mTOR pathway. *Cell Rep*. 2023;42:112779.
26. Gao JF, Zhang L. The role of N^6-methyladenosine (m^6A) in eye diseases. *Mol Biol Rep*. 2021;48:6145–6150.
27. Maminishkis A, Miller SS. Experimental models for study of retinal pigment epithelial physiology and pathophysiology. *J Vis Exp*. 2010;45:2032.
28. Parinot C, Rieu Q, Chatagnon J, Finnemann SC, Nandrot EF. Large-scale purification of porcine or bovine photoreceptor outer segments for phagocytosis assays on retinal pigment epithelial cells. *J Vis Exp*. 2014;94:52100.
29. Almedawar S, Vafia K, Schreiter S, et al. MERTK-dependent ensheathment of photoreceptor outer segments by human pluripotent stem cell-derived retinal pigment epithelium. *Stem Cell Reports*.2020;14:374–389.
30. Moore MJ, Zhang C, Gantman EC, Mele A, Darnell JC, Darnell RB. Mapping Argonaute and conventional RNA-binding protein interactions with RNA at single-nucleotide resolution using HITS-CLIP and CIMS analysis. *Nat Protoc*. 2014;9:263–293.
31. Bailey TL, Johnson J, Grant CE, Noble WS. The MEME suite. *Nucleic Acids Res*. 2015;43:W39–W49.
32. Wingett SW, Andrews S. FastQ Screen: a tool for multi-genome mapping and quality control. *F1000Res*. 2018;7:1338.
33. Dobin A, Davis CA, Schlesinger F, et al. STAR: ultrafast universal RNA-seq aligner. *Bioinformatics*. 2013;29:15–21.
34. Li B, Dewey CN. RSEM: accurate transcript quantification from RNA-Seq data with or without a reference genome. *BMC Bioinformatics*. 2011;12:323.

35. Love MI, Huber W, Anders S. Moderated estimation of fold change and dispersion for RNA-seq data with DESeq2. *Genome Biol*. 2014;15:550.
36. Zhou Y, Zhou B, Pache L, et al. Metascape provides a biologist-oriented resource for the analysis of systems-level datasets. *Nat Commun*. 2019;10:1523.
37. Steinberg RH. Phagocytosis by pigment epithelium of human retinal cones. *Nature*. 1974;252:305–307.
38. Strunnikova NV, Maminishkis A, Barb JJ, et al. Transcriptome analysis and molecular signature of human retinal pigment epithelium. *Hum Mol Genet*. 2010;19:2468–2486.
39. Dominissini D, Moshitch-Moshkovitz S, Schwartz S, et al. Topology of the human and mouse m^{6}A RNA methylomes revealed by m^{6}A-seq. *Nature*. 2012;485:201–206.
40. Yankova E, Blackaby W, Albertella M, et al. Small-molecule inhibition of METTL3 as a strategy against myeloid leukaemia. *Nature*. 2021;593:597–601.
41. Weng H, Huang F, Yu Z, et al. The m^{6}A reader IGF2BP2 regulates glutamine metabolism and represents a therapeutic target in acute myeloid leukemia. *Cancer Cell*. 2022;40:1566–1582.e10.
42. Li H, Ham A, Ma TC, et al. Mitochondrial dysfunction and mitophagy defect triggered by heterozygous GBA mutations. *Autophagy*. 2019;15:113–130.
43. Senabouth A, Daniszewski M, Lidgerwood GE, et al. Transcriptomic and proteomic retinal pigment epithelium signatures of age-related macular degeneration. *Nat Commun*. 2022;13:4233.
44. Liu H, Stepicheva NA, Ghosh S, et al. Reducing Akt2 in retinal pigment epithelial cells causes a compensatory increase in Akt1 and attenuates diabetic retinopathy. *Nat Commun*. 2022;13:6045.
45. Cai J, Litwin C, Cheng R, Ma JX, Chen Y. DARPP32, a target of hyperactive mTORC1 in the retinal pigment epithelium. *Proc Natl Acad Sci USA*. 2022;119:e2207489119.
46. Yin R, Chang J, Li Y, et al. Differential m^{6}A RNA landscapes across hematopoiesis reveal a role for IGF2BP2 in preserving hematopoietic stem cell function. *Cell Stem Cell*. 2022;29:149–159.e7.
47. Peng F, Xu J, Cui B, et al. Oncogenic AURKA-enhanced N^6-methyladenosine modification increases DROSHA mRNA stability to transactivate STC1 in breast cancer stem-like cells. *Cell Res*. 2021;31:345–361.
48. Huang H, Weng H, Sun W, et al. Recognition of RNA N^6-methyladenosine by IGF2BP proteins enhances mRNA stability and translation. *Nat Cell Biol*. 2018;20:285–295.
49. Khristov V, Wan Q, Sharma R, Lotfi M, Maminishkis A, Bharti K. Polarized human retinal pigment epithelium exhibits distinct surface proteome on apical and basal plasma membranes. *Methods Mol Biol*. 2018;1722:223–247.
50. Herm RJ. Age-related macular degeneration. *N Engl J Med*. 2008;359:1735–1736; author reply 1736.
51. Simonelli F, Testa F, de Crecchio G, et al. New *ABCR* mutations and clinical phenotype in Italian patients with Stargardt disease. *Invest Ophthalmol Vis Sci*. 2000;41:892–897.
52. Martin DM, Yee D, Feldman EL. Gene expression of the insulin-like growth factors and their receptors in cultured human retinal pigment epithelial cells. *Brain Res Mol Brain Res*. 1992;12:181–186.
53. Wang Q, Chen Q, Zhao K, Wang L, Wang L, Traboulsi EI. Update on the molecular genetics of retinitis pigmentosa. *Ophthalmic Genet*. 2001;22:133–154.
54. Marmor MF. Mechanisms of fluid accumulation in retinal edema. *Doc Ophthalmol*. 1999;97:239–249.
55. Li J, He J, Zhang X, Li J, Zhao P, Fei P. TSP1 ameliorates age-related macular degeneration by regulating the STAT3-iNOS signaling pathway. *Exp Cell Res*. 2020;388:111811.
56. Newman AM, Gallo NB, Hancox LS, et al. Systems-level analysis of age-related macular degeneration reveals global biomarkers and phenotype-specific functional networks. *Genome Med*. 2012;4:16.
57. Shan K, Zhou RM, Xiang J, et al. FTO regulates ocular angiogenesis via m^{6}A-YTHDF2-dependent mechanism. *Exp Eye Res*. 2020;197:108107.
58. Jia R, Chai P, Wang S, et al. m^{6}A modification suppresses ocular melanoma through modulating *HINT2* mRNA translation. *Mol Cancer*. 2019;18:161.
59. Yao MD, Jiang Q, Ma Y, et al. Role of METTL3-dependent N^6-methyladenosine mRNA modification in the promotion of angiogenesis. *Mol Ther*. 2020;28:2191–2202.
60. Zhu L, Li S, He S, et al. The critical role of m^{6}A methylation in the pathogenesis of Graves' ophthalmopathy. *Eye Vis (Lond)*. 2020;7:55.
61. Zaccara S, Ries RJ, Jaffrey SR. Reading, writing and erasing mRNA methylation. *Nat Rev Mol Cell Biol*. 2019;20:608–624.

Investigative Ophthalmology & Visual Science